

# Anatomy-Aware Conditional Image-Text Retrieval

Meng Zheng<sup>1</sup>, Jiajin Zhang<sup>2\*</sup>, Benjamin Planche<sup>1</sup>, Zhongpai Gao<sup>1</sup>, Terrence Chen<sup>1</sup>, Ziyang Wu<sup>1</sup>  
<sup>1</sup>United Imaging Intelligence, Boston, MA <sup>2</sup>Rensselaer Polytechnic Institute, Troy, NY  
<sup>1</sup>{firstname.lastname}@uii-ai.com, <sup>2</sup>zhangj41@rpi.edu

## Abstract

*Image-Text Retrieval (ITR) finds broad applications in healthcare, aiding clinicians and radiologists by automatically retrieving relevant patient cases in the database given the query image and/or report, for more efficient clinical diagnosis and treatment, especially for rare diseases. However conventional ITR systems typically only rely on global image or text representations for measuring patient image/report similarities, which overlook local distinctiveness across patient cases. This often results in suboptimal retrieval performance. In this paper, we propose an Anatomical Location-Conditioned Image-Text Retrieval (ALC-ITR) framework, which, given a query image and the associated suspicious anatomical region(s), aims to retrieve similar patient cases exhibiting the same disease or symptoms in the same anatomical region. To perform location-conditioned multimodal retrieval, we learn a medical Relevance-Region-Aligned Vision Language (RRA-VL) model with semantic global-level and region-/word-level alignment to produce generalizable, well-aligned multi-modal representations. Additionally, we perform location-conditioned contrastive learning to further utilize cross-pair region-level contrastiveness for improved multi-modal retrieval. We show that our proposed RRA-VL achieves state-of-the-art localization performance in phase-grounding tasks, and satisfying multi-modal retrieval performance with or without location conditioning. Finally, we thoroughly investigate the generalizability and explainability of our proposed ALC-ITR system in providing explanations and preliminary diagnosis reports given retrieved patient cases (conditioned on anatomical regions), with proper off-the-shelf LLM prompts.*

## 1. Introduction

Image-text Retrieval (ITR) has been a widely studied problem in the AI research community [5, 8, 23, 35]. It aims to retrieve relevant images or text from a large database, given a query image or text description. Retrieval tasks have broad

applications, particularly in healthcare [12, 17, 25, 34, 42, 46], supporting clinical diagnosis, treatment planning and disease monitoring, by automatically retrieving and referencing relevant cases from past patient databases. Recently, foundation models like Visual Language Models (VLMs) and Large Language Models (LLMs), have been widely explored in multi-modality (image-text) or cross-modality (image→text or text→image) retrieval tasks [3, 7, 32, 42] due to their superior zero-shot transferability in performing downstream tasks like classification and retrieval, achieved by learning generalizable semantic-aligned textual and visual representations.

Though existing VLM-based solutions have demonstrated satisfactory performance in class-based retrieval tasks in medical domain [3, 19, 45]—*i.e.*, retrieving similar patient cases with the same or similar type(s) of disease given a query medical image or associated report—the performed multi-/cross-modality retrieval primarily relies on global visual or textual report information. This may overlook local anatomical-region-level distinctiveness across patient cases leading to suboptimal retrieval performance, as certain diseases manifest differently depending on their anatomical locations. For instance, a mass in the lung apex might suggest Pancoast tumor, while one near the hilum might indicate metastasis or lymphadenopathy. On the other hand, as lesions typically occupy only small fractions of the image, a global-level retrieval may fail to account for these small region-specific differences, compromising retrieval accuracy.

To overcome these limitations, we propose a novel system that retrieves relevant patient cases showing similar lesion *conditioned on anatomical regions*, providing more effective and efficient diagnosis support to clinicians or radiologists. More specifically, as shown in Figure 1, we explore the problem of anatomical Location-Conditioned Multimodal Retrieval (LC-MMR). Given a query medical image and its region of interest—typically a suspicious anatomical area where radiologists or clinicians have significant uncertainty regarding the presence of a disease—our objective is to retrieve relevant patient cases from the database that exhibit the same or similar conditions *at the same anatomical location*. Furthermore, leveraging the retrieved patient metadata, we

\*This work was done during the internship of Jiajin Zhang at United Imaging Intelligence, Boston, MA.

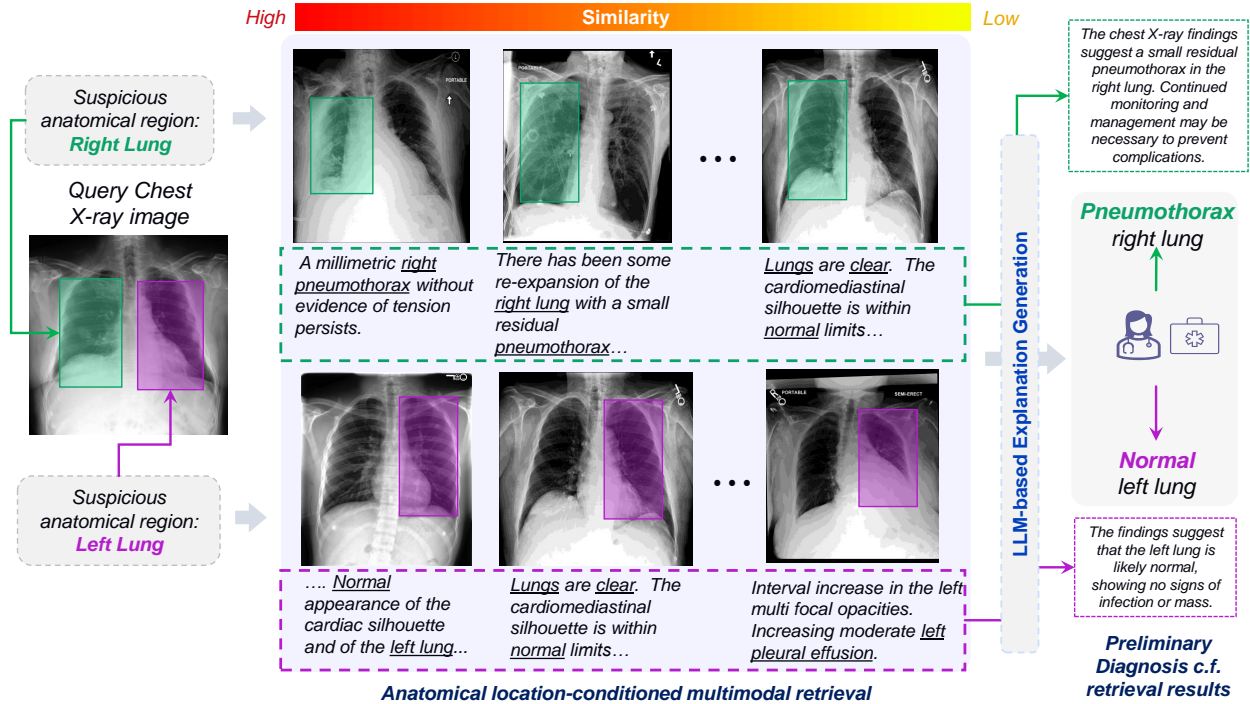


Figure 1. Proposed multimodal retrieval system (ALC-ITR) with anatomical region conditioning. Given a query chest X-ray image and a suspicious anatomical region, our proposed system retrieves the most relevant patient cases showing the same or similar disease, for the same anatomical regions. The system then prompts LLMs based on retrieval results for explanation generation and preliminary diagnosis.

prompt general LLMs (without domain-specific fine-tuning) to generate explanations and provide a preliminary diagnosis for the query case at the anatomical region level.

To develop an effective system for location-conditioned retrieval (LC-MMR), directly applying existing medical VLM solutions [3, 19, 45] trained on image-report pairs is suboptimal. These models optimize a shared embedding space mapped from *global* visual and textual features, lacking explicit location conditioning. As a result, they may fail to capture critical regional relevance information, which is essential for the proposed LC-MMR task. While numerous works have been proposed [6, 9, 19, 26, 31, 39] to improve the granularity of visual-textual alignment for better multi-modal representation learning, they are essentially learning global representations with vague region-level information. They are designed for specific downstream applications such as image classification, report generation, or pathology recognition; and thus do not properly transfer to LC-MMR.

To this end, we propose to learn a weakly-supervised region-relevance-aligned biomedical Vision Language (RRA-VL) model for LC-MMR. Specifically we focus on chest X-Ray (CXR) images paired with radiology reports; leveraging MIMIC-III/CXR [22], a large-scale, multi-modal dataset with disease-level annotations which is well-suitable for our study. In addition to semantic global alignment, we extend RRA-VL with a novel region-/word-level visual-

textual alignment module performing residual-connected intra- and cross-modality attention to enforce local alignment between medical images and reports. Furthermore, we enforce a location-conditioned contrastive learning loss, utilizing patient case distinctiveness at lesion level for improved multi-modal retrieval. We show that our proposed RRA-VL enables LC-MMR and can achieve greater retrieval performance with location-informed contrastive learning. We further demonstrate the lesion-level explainability of proposed ALC-ITR system in providing diagnosis suggestions given retrieved patient case gallery, which facilitates more comprehensive patient case understanding and interpretation.

To summarize, our contributions are listed as follows:

- We introduce a novel Anatomical Location-Conditioned Image-Text Retrieval system (ALC-ITR), which is able to retrieve similar patient cases with same disease or symptoms *conditioned on anatomical locations*, enabling patient case understanding and diagnosis support at finer level compared to conventional medical retrieval system.
- We propose a weakly-supervised region-relevance-aligned medical Vision Language (RRA-VL) model, with attentive region-/word-level and global semantic alignment for generalizable multi-modal representation learning. We further enforce a location-conditioned triplet mining loss for RRA-VL learning, resulting in improved multi-modal retrieval performance.

- Our proposed ALC-ITR system enables region-level explainability and provides preliminary diagnosis at anatomical locations, without requiring specific text generator learned with domain-specific knowledge and annotations.
- We demonstrate the superior multi-modal representation learning capability of the proposed RRA-VL on various downstream tasks, including phase-grounding, multi-modality retrieval with/without location conditioning. The proposed RRA-VL achieves state-of-the-art phase-grounding and satisfying multi-modal retrieval performance compared to existing solutions.

## 2. Related Work

### 2.1. Medical Vision-Language Model

With the ongoing development of Foundation Models, much effort has been put in learning generalizable Vision Language Models (VLMs) from large-scale paired image-text data [15, 18, 24, 29, 37, 40]. Common approaches typically enforce contrastive objectives on CLIP-like architectures [36] to learn a joint visual-textual embedding space. Training medical VLMs remains, however, challenging; as public medical image-report paired datasets are in much smaller scale than in-the-wild image-text datasets such as LAION-5B [38], COYO-700M [4] *etc.* Numerous works have been proposed [3, 6, 9, 19, 26, 30, 31, 39, 44] to learn more generalizable visual-textual representation for medical data, by enforcing different levels of vision-language alignment during large-scale pretraining. While some are aiming at learning generic multi-modal representations [9, 19, 26, 30, 39, 44], others are specifically curated for different downstream tasks, *e.g.*, report generation [6, 41], which may not easily translate to the proposed location-conditioned image/text retrieval (LC-MMR) problem. In this paper, we propose a novel attentive word-region-level local alignment scheme enforced with semantically weighted cross-modality consistency. We show that the proposed alignment scheme achieves superior localization capability in phase grounding tasks compared to existing solutions, while enabling LC-MMR with explicit region conditioning.

### 2.2. Image-Text Retrieval

Image-text retrieval is a rapidly advancing AI research area that focuses on developing methods to retrieve relevant information across modalities, such as finding an image based on a textual query or vice versa. We refer the readers to [5] for a detailed survey on image-text retrieval. Conventional image or text retrieval refers to category/class-level retrieval, *i.e.*, the retrieval of candidates in a database which share the same category as the query. Existing approaches [19, 44, 47] typically leverages global similarities between image and/or text features for retrieval. We argue that local distinctiveness across different patient cases is crucial and should be

utilized for more accurate and specialized retrieval particularly in medical domain. Specifically, we extend existing multi-modal (image-text) retrieval systems and propose a novel anatomical location-conditioned image-text retrieval (ALC-ITR) system, which retrieves relevant patient cases conditioned on anatomical regions, given the query radiology image and suspicious anatomical location(s). This further facilitates finer-level interpretability of a medical retrieval system by querying an image at various anatomical regions, and providing explanations and preliminary diagnosis accordingly based on region-level visual similarities.

## 3. Method

To learn our proposed Region-Relevance-Aligned Vision Language (RRA-VL) model for Location-Conditioned Multimodal Retrieval (LC-MMR), we first achieve global and local semantic alignment of the image and text representations at multi-granularity levels in an unsupervised manner (Section 3.1). We then perform location-conditioned contrastive learning given disease labels as weak supervision for improved LC-MMR (Section 3.2). We finally investigate the explainability of the proposed Anatomical Location-Conditioned Image-Text Retrieval (ALC-ITR) system in Section 3.3. The overall pipeline is illustrated in Figure 2.

### 3.1. VLM Learning with Global/Local Alignment

#### 3.1.1. Feature Extraction

Given a radiology image  $I_i$ , *e.g.* a chest X-ray (CXR) image, along with its radiology report  $T_i$ , we adopt a ResNet-50 [16] as the image encoder,  $E_I$ , and a BERT model [43] as the text encoder  $E_T$ , according to conventional medical vision-language model (VLM) frameworks [3, 9, 19]. Specifically, the image encoder takes in the CXR image  $I_i$  and outputs a grid of local patch embeddings  $\mathbf{f}_i^P$  of size  $c \times w \times h$ . The text encoder takes in the radiology report  $T_i$  (paired with CXR image  $I_i$ ) and generates a list of token representations  $\mathbf{t}_i$ . The local image patch embeddings and the textual token representations are then utilized for cross-modality alignment, as elaborated next.

#### 3.1.2. Global Alignment

To globally align image and textual representations, we first project local patch embeddings  $\mathbf{f}_i^P$  to  $\hat{\mathbf{f}}_i^P$  and average-pool them to generate projected global image embedding  $\hat{\mathbf{f}}_i^G$ . We then project the first [CLS] token,  $\mathbf{t}_i^C$ , of the sequence token representations  $\mathbf{t}_i$  into the shared image-text embedding space and generate  $\hat{\mathbf{t}}_i^C$  as global textual representation. We then follow a contrastive-learning strategy [3, 19, 44] to apply symmetric alignment loss to semantically align global

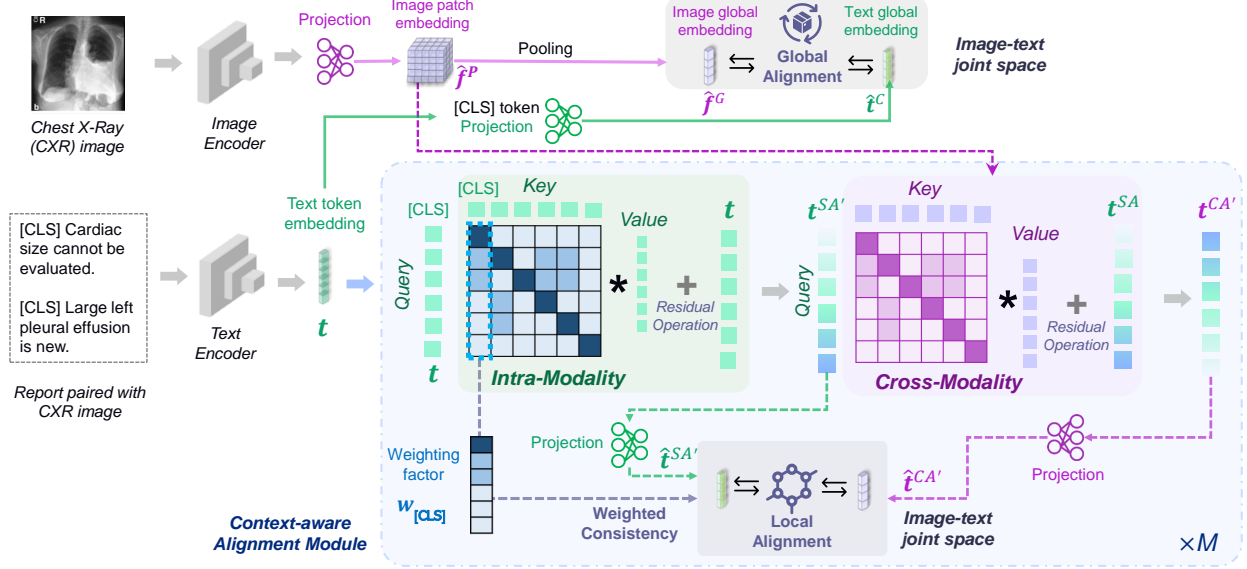


Figure 2. Proposed Region-Relevance-Aligned medical Vision Language (RRA-VL) model with global and local alignment.

image and text features:

$$\mathcal{L}_G = -\frac{1}{N} \sum_{i=1}^N \left( \log \frac{\exp(\hat{f}_i^G \cdot \hat{t}_i^C / \tau_G)}{\sum_{j=1}^N \exp(\hat{f}_i^G \cdot \hat{t}_j^C / \tau_G)} + \log \frac{\exp(\hat{t}_i^C \cdot \hat{f}_i^G / \tau_G)}{\sum_{j=1}^N \exp(\hat{t}_i^C \cdot \hat{f}_j^G / \tau_G)} \right), \quad (1)$$

where  $N$  is the number of image-text pairs in a training batch,  $\tau_G$  is the scaling temperature parameter, and  $\hat{f}_i^G \cdot \hat{t}_j^C$  is the cosine similarity between global image  $\hat{f}_i^G$  and textual embedding  $\hat{t}_j^C$ .

### 3.1.3. Local Alignment

While global alignment with  $\mathcal{L}_G$  semantically reconcile image and text representations, region-/word-level lesion-report association with finer granularity is crucial to localization-related downstream tasks like grounding and the proposed LC-MMR [3, 9, 19, 26, 30, 31, 44]. To this end, we propose a Context-Aware Alignment (CAA) module consisting of intra-modality and cross-modality correspondence learning in a cascaded way.

Specifically, given the sequence of token representations  $t_i$  generated by the text encoder from the input report  $T_i$  (Section 3.1.1), we first enforce self-attention [11] by computing the Multi-Head Attention (MHA) [43] where each token attends to every other token in the sequence, to capture intra-sequence relationships and highlight informative word tokens and generate initial self-attentive token features  $t_i^{SA}$ :

$$t_i^{SA} = \text{Softmax} \left( \sqrt{\frac{1}{d_k}} W_s^q t_i \cdot W_s^k t_i \right) W_s^v t_i, \quad (2)$$

where  $W_s^q$ ,  $W_s^k$  and  $W_s^v$  are learnable weight matrices specific to each attention head. We then perform a residual

operation to compute final self-attentive token features as:  $t_i^{SA'} = t_i^{SA} + t_i$ .

To align local representations across image and text modalities, we perform cross-attention with MHA by querying self-attentive token features  $t_i^{SA'}$  with image patch features  $\hat{f}_i^P$ , to generate initial cross-attentive/modality token features  $t_i^{CA}$  as:

$$t_i^{CA} = \text{Softmax} \left( \sqrt{\frac{1}{d_k}} W_c^q t_i^{SA'} \cdot W_c^k \hat{f}_i^P \right) W_c^v \hat{f}_i^P. \quad (3)$$

Similarly,  $W_c^q$ ,  $W_c^k$  and  $W_c^v$  are learnable weight matrices specific to each attention head. The residual operation is then performed to obtain final cross-modality token features,  $t_i^{CA'} = t_i^{CA} + t_i^{SA'}$ , for subsequent computations.

We subsequently project cross-modality token features and self-attentive token features to image-text joint space:  $t_i^{CA'} \rightarrow \hat{t}_i^{CA'}$ ,  $t_i^{SA'} \rightarrow \hat{t}_i^{SA'}$ . Then we compute the local alignment loss to enforce *weighted consistency* between intra-modality and inter-modality feature representations. Specifically, we adopt [CLS] token attention weights  $w_{[CLS]}$  (the attention scores when [CLS] token attends to other tokens in the sequence) to suppress less meaningful words in our application context (e.g., ‘‘a’’, ‘‘is’’) and highlight informative local descriptions (e.g., ‘‘pleural effusion’’), for targeted context-aware local alignment:

$$\mathcal{L}_l = -\frac{1}{N} \sum_{i=1}^N \left\{ \log \frac{\exp[w_{[CLS]} \circ (\hat{t}_i^{SA'} \cdot \hat{t}_i^{CA'} / \tau_L)]}{\sum_{j=1}^N \exp[w_{[CLS]} \circ (\hat{t}_i^{SA'} \cdot \hat{t}_j^{CA'} / \tau_L)]} + \log \frac{\exp[w_{[CLS]} \circ (\hat{t}_i^{CA'} \cdot \hat{t}_i^{SA'} / \tau_L)]}{\sum_{j=1}^N \exp[w_{[CLS]} \circ (\hat{t}_i^{CA'} \cdot \hat{t}_j^{SA'} / \tau_L)]} \right\}. \quad (4)$$

Similar to Equation 1,  $N$  is the number of image-report pair in a training batch,  $\tau_L$  is the scaling temperature parameter. ‘‘ $\circ$ ’’ is the cosine similarity operator, and ‘‘ $\circ$ ’’ denotes

Hadamard product. The Context-Aware Alignment (CAA) module is repeated  $M$  times to compute the final multi-modal feature representations ( $M = 3$  in our implementation, *c.f.* supplementary material for detailed discussions).

### 3.2. Location-conditioned Contrastive Learning

While global and local alignment mechanisms introduced in Section 3.1 align visual and textual representations across different granularity levels, intra-pair contrastiveness is not fully explored during the unsupervised learning process. This may result in suboptimal performance in downstream tasks like classification or retrieval. One may perform conventional contrastive learning given disease labels (typically accessible for CXR datasets) to overcome this limitation, *i.e.*, constructing positive and negative pairs with patient data labeled with same or different diseases. However, disease-level contrastive learning based on global image/text features bring further challenges, considering that: 1) medical data is typically multi-label data, *i.e.*, a patient may commonly have concurrent diseases happening at different anatomical regions, so constructing positive/negative data pairs solely based on disease categories can easily confuse the model and compromise its performance; 2) lesions commonly span over tiny regions of a medical image, so contrastive learning based on global representations without explicit region-/location-conditioning is not optimal for accurate retrieval and query case understanding.

To this end, we propose to enforce local/regional contrastive learning based on region-level disease labels as weak supervision, for improved location-conditioned retrieval (LC-MMR) performance. However, existing CXR datasets either contain only image-level disease labels without explicit region annotations like bounding boxes or segmentation masks [10, 20, 22]; or have too few of them [3], which may easily cause model overfitting and are thus not optimal for our study. Therefore, we propose to use general LLMs, *i.e.*, GPT-4o [1] to preprocess MIMIC-III/CXR [22] data and extract region-level information from the radiology reports. Specifically, we use GPT-4o to extract anatomical region information and corresponding symptom/disease descriptions from the report. *E.g.*, a CXR image with report stating “linear opacity at the right lung base is suggestive of subsegmental atelectasis”. “right lung base” and “subsegmental atelectasis” are extracted as the region and disease descriptions respectively. We then form triplets based on region and disease labels, with positive pairs constructed as samples showing same symptom/disease at same anatomical region and negative pairs otherwise (different symptoms/diseases at same region or different symptoms/diseases at different regions, *c.f.* supplementary material Section 1 for more detailed discussions). To enforce regional contrastive learning, we input the CXR images and region descriptions into the image and text encoders to generate region-conditioned

cross-attentive features and minimize the triplet loss on positive/negative pairs as:

$$\mathcal{L}_{tr} = \frac{1}{N} \sum_{i=1}^N \max(\ell_2(\hat{\mathbf{t}}_i^a, \hat{\mathbf{t}}_i^p) - \ell_2(\hat{\mathbf{t}}_i^a, \hat{\mathbf{t}}_i^n) + \alpha, 0). \quad (5)$$

Here  $N$  is the total number of triplet pairs in a sampled batch,  $\alpha$  is the predefined margin hyperparameter, and  $\hat{\mathbf{t}}_i^a, \hat{\mathbf{t}}_i^p, \hat{\mathbf{t}}_i^n$  correspond to the cross-attentive feature vectors (*i.e.*,  $\hat{\mathbf{t}}_i^{\text{SA}'}$ ) from the context-aware alignment module, respectively for the anchor, positive, and negative samples for triplet  $i$ .

### 3.3. Overall Training and Interpretability

We perform a two-stage training to learn our proposed RRA-VL. *I.e.*, we first finetune RRA-VL with global alignment loss and local alignment loss (Section 3.1) as  $\mathcal{L}_a = \mathcal{L}_G + \beta\mathcal{L}_l$ , on MIMIC-III/CXR [22] dataset. We then train RRA-VL with  $\mathcal{L}_{tr}$  on processed MIMIC-III/CXR dataset (as illustrated in Section 3.2) with location-conditioned triplet pairs as the input to RRA-VL to enforce regional contrastive learning. Dense annotations, *e.g.*, bounding boxes or segmentation masks, are not required for training our RRA-VL. Refer to Section 4.1 and supplementary material for additional implementation details.

Given a query CXR image and the suspicious anatomical region(s), our proposed ALC-ITR pipeline can effectively retrieve similar cases from database conditioned on the querying region, interpretations and explanations can thus be automatically generated by referring to the retrieved patient gallery, as shown in Figure 3. Specifically, given the retrieved gallery with patients’ metadata (including CXR image-report pairs) ranked with region-level similarities, we leverage LLMs (GPT-4o-mini [1] in this example) to generate explanations given retrieved top- $k$  similar case(s) based on their regional disease descriptions. *E.g.*, our proposed ALC-ITR system retrieves a patient gallery given the query image in Figure 3, when conditioned on suspicious anatomical region “heart”. We then prompt LLMs with the top- $k$  ( $k=1$  in Figure 3 for illustration purpose) patient report(s) to generate explanations and preliminary diagnosis. Ground-truth reports of the query image can then be utilized for evaluations, which will be illustrated in Section 4.4.

## 4. Experiments

To evaluate the efficacy of our proposed ALC-ITR system, we first validate the representation capability of the learned multi-modal visual-textual embedding by demonstrating state-of-the-art localization performance of our RRA-VL model on phase grounding tasks. We then demonstrate the capability of ALC-ITR in performing Location-Conditioned Multi-Modal Retrieval (LC-MMR), as well as conventional cross-modality retrieval tasks, showing superior accuracy when compared to existing medical VLM solutions.

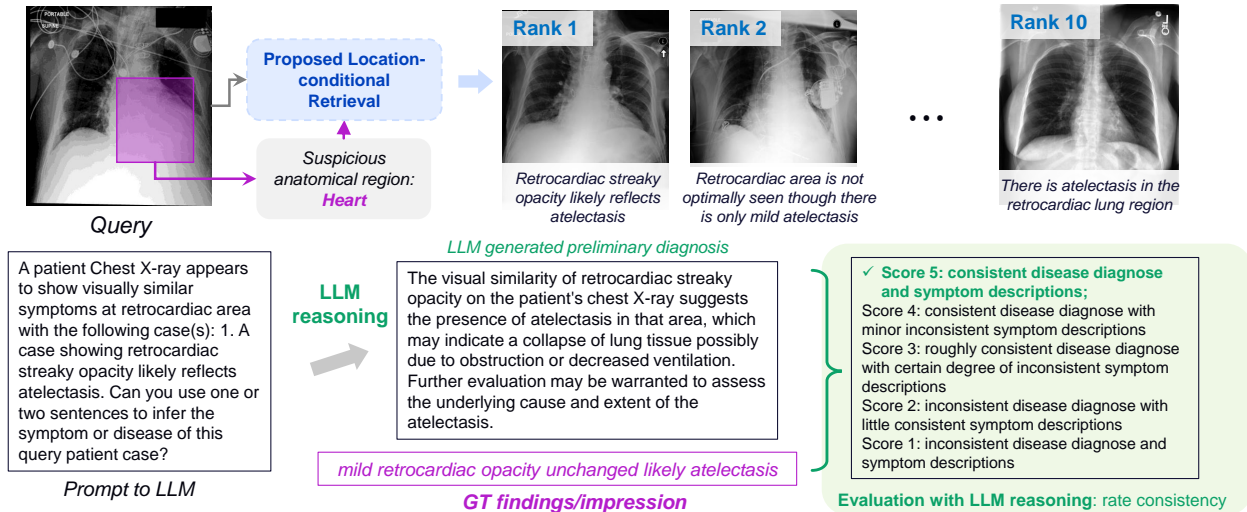


Figure 3. Proposed explanation generation pipeline based on location-conditioned multi-modal retrieval. Upper part shows retrieved patient gallery given the query image conditioned on “Heart” region. Bottom part illustrates the explanation generation and evaluation pipeline.

We finally study and evaluate explainability of the proposed ALC-ITR compared to conventional image-text retrieval system. Implementation details and additional experimental results can be found in the supplementary material.

#### 4.1. Experimental Protocol

**Datasets.** a) **MIMIC-III/CXR.** We perform first-stage training on MIMIC-III/CXR [22] training set. b) **MIMIC-loc.** For second-stage training of RRA-VL, we preprocess original MIMIC-III/CXR dataset to extract region-level disease descriptions as illustrated in Section 3.3, and generate 15.9k/2.1k training/testing data samples with meaningful regional disease descriptions from MIMIC-III/CXR training/testing samples. We refer to our re-curated MIMIC-III/CXR dataset as MIMIC-loc in the following context for easier differentiation. MIMIC-loc will be made publicly available upon acceptance of this paper. c) **MS-CXR.** For evaluation of the finegrained localization performance of proposed RRA-VL model, we perform phase grounding tasks on MS-CXR [3]. MS-CXR has local image region (bounding box) annotations with descriptions of eight radiology findings of 1,153 data samples, curated from MIMIC-III/CXR dataset. d) **CheXpert 5x200.** To evaluate the multi-modal representation capability of learned RRA-VL on conventional class-based image-report retrieval task, *i.e.*, given an query image, the accuracy of retrieved reports belong to the same category (disease) as the query image; and given a query report, the accuracy of retrieved images belong to the same category as the query report for report-image retrieval. We perform cross-domain retrieval evaluation on CheXpert 5x200 dataset. CheXpert 5x200 dataset is re-curated from CheXpert [20], which contains 200 exclusively positive images for each of category: atelectasis, cardiomegaly, con-

solidation, edema and pleural effusion, to avoid multi-label confusions for retrieval tasks. Please note that we do not train on CheXpert/CheXpert 5x200 dataset but only perform cross-domain evaluations to validate the generalizability of the learned multi-modal representations of RRA-VL.

**Metrics** For phase grounding, we follow [3, 9] and use mean Intersection over Union (mIoU) and Contrast-to-noise ratio (CNR) for evaluating localization accuracy. We use Rank@K [9, 19, 44] to measure the percentage of top- $k$  retrieved items are correct matches for retrieval tasks and mean Average Precision (mAP) to evaluate ranking quality across all retrieved results.

#### 4.2. Phase Grounding Evaluation

**Comparison to State-of-the-art.** To evaluate the localization capability of the proposed RRA-VL model, we perform phase grounding evaluation on MS-CXR [3], strictly following protocol proposed in [3]. Specifically for each testing image-report pair in MS-CXR dataset, we input CXR image and corresponding phase descriptions to RRA-VL and compute cosine similarities between projected image patch embeddings  $\hat{\mathbf{f}}^P$  and cross-modality text features  $\hat{\mathbf{t}}^{CA}$  to generate the similarity maps. We then upsample these maps to the original CXR image size [14] and compare with the ground-truth bounding-box annotations for mIoU and CNR calculations. Results presented in Table 1 and 2 confirm that the proposed RRA-VL achieves superior phase grounding accuracy in terms of both mIoU and CNR compared to existing methods, demonstrating its strong multimodal representation capability benefited from the proposed multi-granularity alignment learning scheme. Visualizations are presented in Figure 4.

**Ablation Study.** We evaluate the role of global alignment

Table 1. Comparison of proposed RRA-VL to prior arts, evaluated by per-category Contrast-to-noise ratio (CNR) on MS-CXR [3] dataset.

Methods	Atelectasis	Cardiomegaly	Consolidation	Lung opacity	Edema	Pneumonia	Pneumothorax	Pl. effusion	Avg.
ConVIRT [47]	0.86±.04	0.64±.06	1.25±.06	0.78±.07	0.68±.07	1.03±.05	0.28±.08	1.02±.03	0.818±.01
GLoRIA [19]	0.98±.04	0.53±.31	1.38±.03	1.05±.04	0.66±.03	1.18±.04	0.47±.02	1.20±.04	0.930±.03
BioViL [3]	1.02±.06	0.63±.08	1.42±.02	1.05±.06	0.93±.03	1.27±.04	0.48±.06	1.40±.06	1.027±.02
BioViL-L [3]	1.17±.04	0.95±.21	1.45±.03	1.19±.05	0.96±.05	1.19±.01	0.74±.05	<b>1.50±.03</b>	1.142±.04
LIMITR [9]	1.16±n/a	<b>1.18±n/a</b>	1.37±n/a	1.37±n/a	1.05±n/a	1.27±n/a	1.01±n/a	1.24±n/a	1.206±n/a
<b>RRA-VL(ours)</b>	<b>1.48±.01</b>	1.07±.01	<b>1.58±.02</b>	<b>1.51±.04</b>	<b>1.15±.04</b>	<b>1.41±.01</b>	<b>0.95±.03</b>	1.40±.04	<b>1.333±.03</b>

Table 2. Phase grouping performance comparison of RRA-VL to state-of-the-art on MS-CXR [3] dataset. Results are averaged over five runs with different random seeds following [3].

Methods	Venues	mIoU	CNR
Clinical-BERT [2]	ClinicalNLP 2019	0.182	0.791
BioViL [3]	ECCV 2022	0.194	0.796
ConVIRT [47]	ML Healthcare 2022	-	0.818
BioViL+MLM [3]	ECCV 2022	0.209	0.860
GLoRIA [19]	ICCV 2021	-	0.930
BioViL+dropout [3]	ECCV 2022	0.217	0.945
BioViL+RSM [3]	ECCV 2022	0.220	1.012
BioViL+CXR-BERT [3]	ECCV 2022	0.220	1.031
<b>RRA-VL(ours)</b>	-	<b>0.348</b>	<b>1.276</b>

Table 3. Ablation study of RRA-VL on MS-CXR [3], evaluated on phase grounding tasks.

Global	Local			mIoU	CNR
	Intra-Modality	Cross-Modality			
		+Residual	+w <sub>[CLS]</sub>		
✗	✗	✗	✗	0.246	1.014
✓	✗	✗	✗	0.279	1.178
✗	✓	✓	✓	0.305	1.255
✓	✓	✗	✗	0.293	1.249
✓	✓	✓	✗	0.323	1.272
✓	✓	✗	✓	0.319	1.281
✓	✓	✓	✓	<b>0.350</b>	<b>1.283</b>

and the context-aware alignment module including the intra-modality and inter-modality correspondence learning. From the ablation study shared in Table 3, we observe that context-aware local alignment brings larger benefits compared to global alignment to the phase grounding performance, with residual operations (“+Residual”) and weighted consistency (“+w<sub>[CLS]</sub>”) further improving localization accuracy.

### 4.3. Multimodal Retrieval Evaluations

**Location-conditioned Multimodal Retrieval (LC-MMR).** To validate the proposed RRA-VL in performing LC-MMR, we input each CXR image and anatomical location descriptions in MIMIC-loc testing set, to our proposed RRA-VL to generate cross-modality text embeddings  $\hat{\mathbf{t}}^{CA}$  as multimodal embeddings for the target retrieval task. Note that for each testing query image, we only perform retrieval at anatomical region(s) where disease(s) exist, *i.e.*, where the

ground-truth disease labels are positive, for evaluation purposes. We evaluated Rank@K and mAP of RRA-VL for LC-MMR, under two settings in Table 4. “Region-level” retrieval refers to the scenarios when a retrieved CXR data is counted as a correct match for Rank@K evaluation if both anatomical location and disease category are the same as the query data. “Image/global-level” refers to a more relaxed setting where the retrieved items are counted as correct as long as the disease category is consistent with the query, no matter the anatomical regions. To the best of our knowledge, this is the first proposed pipeline for LC-MMR, and as such, it lacks baselines for performance comparison. To ensure a fair evaluation, we conduct the same experiments using publicly accessible BioViL [3] checkpoints. We show that the proposed RRA-VL achieves significantly better LC-MMR performance compared to BioViL [3]. On the other hand, Table 4 shows that proposed RRA-VL achieves satisfying retrieval performance with alignment loss only (“w/o  $\mathcal{L}_{tr}$ ”), with further performance improvement when location-conditioned triplet mining is added. This aligns with the expectation that the proposed alignment scheme enforces context-aware multimodal representation learning, which enables LC-MMR, with regional contrastive learning further boosts LC-MMR performance.

**Conventional Class-based Retrieval.** To evaluate the generalizability of proposed RRA-VL for conventional cross-modality retrieval, we report Rank@K Image2Report and Report2Image retrieval performance on CheXpert 5x200 [19, 20, 47] dataset in cross-domain setting. Table 5 shows the proposed RRA-VL can achieves better Image2Report retrieval accuracy with large margin *c.f.* Rank@5 and Rank@10 metric, with on-par Report2Image retrieval performance compared to BioViL [3]. Additional in-domain retrieval evaluation can be found in supplementary material.

### 4.4. Explainability

As illustrated in Section 3.3, our proposed ALC-ITR pipeline naturally offers finer-level explainability, thanks to its capability in enabling retrieval conditioned at different anatomical regions. To evaluate the quality of generated preliminary diagnosis and explanations for each query case, we input the generated descriptions from LLMs and ground-truth region-level descriptions (available in MIMIC-loc dataset, *c.f.* Section 4.1), and prompt LLMs to

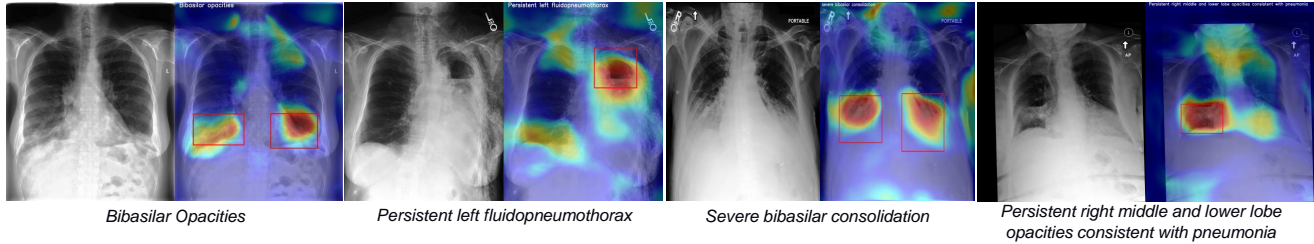


Figure 4. Visualization of phase grounding heatmaps of proposed RRA-VL on MS-CXR [3]. Red boxes are ground-truth bounding boxes.

Table 4. Class-based location-conditioned multi-modal retrieval evaluation of RRA-VL on MIMIC-loc test set.

Methods	Region-level				Image/Global-level				
	Rank@1	Rank@5	Rank@10	mAP	Rank@1	Rank@5	Rank@10	mAP	
BioViL [3]	11.58	40.68	57.53	9.66	23.95	65.58	83.68	20.04	
<b>RRA-VL (ours)</b>	w/o $\mathcal{L}_{tr}$	61.63	82.16	87.47	45.37	65.74	86.11	91.16	45.86
	w. $\mathcal{L}_{tr}$	65.11	84.37	89.00	51.92	67.95	86.74	91.79	53.43

Table 5. Class-based retrieval evaluation of RRA-VL on CheXpert 5x200 dataset [19, 47] (cross-domain evaluation).

Methods		Rank@1	Rank@5	Rank@10
Image2Report	BioViL [3]	19.94	51.30	59.52
	<b>RRA-VL (ours)</b>	<b>20.44</b>	<b>61.32</b>	<b>98.90</b>
Report2Image	BioViL [3]	<b>24.55</b>	69.14	86.67
	<b>RRA-VL (ours)</b>	20.54	<b>72.65</b>	<b>91.68</b>

rate a consistency score between them in the scale of 1-5 (Figure 3 bottom part and supplementary material gives a detailed explanation of the evaluation process and the metric definition of score 1-5). Figure 5 presents the average consistency score rated by GPT-4o-mini under 3 settings, “Proposed” refers to the case where we use the top-1 retrieved patient report from proposed ALC-ITR system to generate explanations and compared to ground-truth regional disease/symptom descriptions. “Baseline” is similar to “Proposed” but relies on global image representations instead of cross-attentive multi-modal features from RRA-VL to perform retrieval and generate patient gallery (subsequent explanation generation and evaluation are the same as “Proposed”). “Pseudo-GT” refers to the scenario where we use ground-truth top-1 match (as the retrieved top-1 match may not always be correct) to generate explanations and evaluate the consistency score accordingly. From Figure 5, we can see that global-level retrieval (“Baseline”) results in lower consistency scores with an average score of 2.40. This reflects the limitations of conventional global-level retrieval without explicit anatomical region conditioning, where inaccurate preliminary diagnosis may be generated due to suboptimal retrieval accuracy. On the other hand, our proposed ALC-ITR pipeline (“Proposed”) can generate reasonable explanations with average score 3.22, with small margin of degradation compared to “Pseudo-GT”, due to retrieval imperfection.

#### Discussion: Comparison to Image Report Generation.

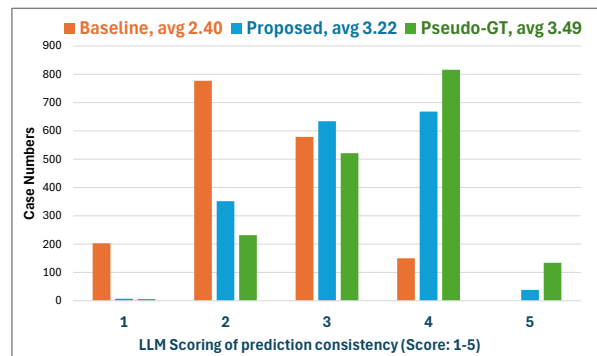


Figure 5. Statistics of rated consistency score (GPT-4o-mini) of generated explanations and GT descriptions, conditioned at different anatomical regions. Evaluation protocol is described in Figure 3.

Conventional image report generation aims to generate a comprehensive report given a CXR image, and existing pipelines typically require finetuned/retrained text generators [6, 31] with in-domain knowledge and full radiology reports as supervision. This can potentially lead to model overfitting with seen diseases and data modalities. Compared to image report generation pipelines, our proposed ALC-ITR system can generate region-level disease or symptom descriptions without requiring any domain-specific text generator (only general LLMs like GPT-4o-mini), instead based on regional similarity/dissimilarity. As a result, our ALC-ITR system is more flexible, and potentially more generalizable to unseen data and diseases.

## 5. Conclusion

We propose an anatomical location-conditioned image-text retrieval (ALC-ITR) system, to retrieve relevant patient cases given query CXR image conditioned on anatomical region similarities. To perform ALC-ITR, we propose to



learn a weakly-supervised RRA-VL model with novel multi-granularity alignment and location-conditioned contrastive learning. Our proposed  $\text{ALC-ITR}$  system is able to learn generalizable, well-aligned multimodal representations with superior localization capability, while enabling location-conditioned multimodal retrieval with fine explainability.

# Supplementary Material

## 1. Implementation Details

**Architecture** We adopt ResNet-50 [16] as our image encoder and BERT [11, 43] as our text encoder, initialized with weights pretrained from BioViL [3] following conventional multi-modal learning schemes [19].

**Training** We perform a two-stage training scheme as introduced in Section 3.3 in the main paper. Specifically, for first-stage learning, we input “IMPRESSION” and “FINDINGS” sections of a CXR report to the text encoder along with the CXR image (posteroanterior, PA view only) to the image encoder following similar strategy in [3, 33], as “IMPRESSION” and “FINDINGS” sections of a CXR report typically contain detailed information of radiological interpretations from the radiologist. During second-stage training of RRA-VL, triplet pairs are generated online (*c.f.* Section 3.3 in our main paper) given location description and disease category labels. Note that normal cases can be paired with normal/abnormal cases as positive/negative pair, regardless of the conditioning anatomical region. A figure illustration of the triplet sampling process can be found in Figure 6.

**Hyperparameters** We adopt AdamW optimizer [28] with learning rate  $5e^{-6}$ , weight decay 0.01,  $\beta = 0.1$  (*c.f.* Section 3.3 in the main paper) for training our context-aware alignment (CAA) module. We use Adam optimizer with learning rate  $5e^{-6}$ , weight decay  $1e^{-5}$  for finetuning the image and text encoder. Total training epoch is set to 10. We resize and center crop images to  $512 \times 512$  and perform random horizontal flips as image augmentations. We empirically set  $M = 3$  (*c.f.* Section 3.1 in the main paper) as we found that  $M = 3$  compromise the best between convergence and computation efficiency for CAA (model learning does not converge when  $M < 3$ , while increasing  $M$  does not improve performance on the other hand).

**Evaluation with LLM Reasoning** For evaluation of consistency between generated explanations and ground-truth disease/symptom descriptions for each query (workflow illustrated in right bottom part of Figure 3 with experimental results shown in Figure 5), we prompt GPT-4o-mini with the following statement: “Can you rate the consistency of the following two descriptions of a patient X-ray report in a scale of 1-5? Score 1 represents completely inconsistent disease diagnose and symptom descriptions. Score 2 represents inconsistent disease diagnose with little consistent symptom descriptions. Score 3 represents roughly consistent disease diagnose with certain degree of inconsistent symptom descriptions. Score 4 represents consistent disease diagnose with some inconsistent symptom descriptions. Score 5 represents completely consistent disease diagnose and symptom descriptions. Following are the two descriptions: A.

(generated explanations). B. (ground-truth disease/symptom descriptions)”. We then collect the returned score from GPT-4o-mini as the final rated consistency score for the query.

## 2. In-Domain Multimodal Retrieval Results

To demonstrate the capability of proposed RRA-VL in performing conventional cross-modality retrieval. We follow protocol proposed in [9, 19] and perform in-domain cross-modality retrieval on MIMIC-III/CXR test set and compare to existing medical VLM solutions. Specifically we perform cosine similarities between global image features  $\hat{f}^G$  and cross-attentive token features  $t^{CA}$  (*c.f.* Figure 2 in the main paper) given CXR images and reports to rank similarities and obtain retrieval results. “Image2Report” refers to cases where reports are being retrieved given query images, while “Report2Image” denotes cases where images are being retrieved given query reports. We report Rank@1, Rank@5 and Rank@10, and calculate the percentage of queries whose correct matches are successfully ranked within top-1, 5 and 10 in Table 6. Table 6 demonstrates that our proposed RRA-VL achieves state-of-the-art Rank@5 and Rank@10 with noticeable margin for both Image-Report retrieval and Report-Image retrieval.

Table 6. In-domain multimodal retrieval evaluation of RRA-VL on MIMIC-III dataset [22], compared to prior arts.

Methods	Image2Report			Report2Image		
	R@1	R@5	R@10	R@1	R@5	R@10
MOTOR [27]	10.96	31.93	42.90	12.00	33.10	44.32
Im2Cap [13]	18.60	43.10	56.10	18.13	43.20	55.97
JolmTeR-Net [21]	18.93	46.20	58.67	19.07	45.27	58.50
MGCA [44]	25.80	51.90	62.10	27.90	51.20	61.60
ConVIRT [47]	30.10	53.90	63.80	29.20	54.70	64.40
GLoRIA [19]	30.30	57.50	66.50	24.00	51.80	62.80
LIMITR [9]	36.10	59.10	69.10	36.40	60.70	70.50
LIMITR(+LT&PE) [9]	<b>39.70</b>	63.20	71.70	37.70	62.10	71.30
<b>RRA-VL (ours)</b>	38.64	<b>74.27</b>	<b>82.60</b>	<b>39.94</b>	<b>62.86</b>	<b>86.39</b>

## 3. Additional Visualizations

### 3.1. Phase Grounding

We show additional visualizations of phase grounding heatmaps (corresponding to Figure 4 in the main paper) of proposed RRA-VL on MS-CXR [3] in Figure 7 and Figure 8.

### 3.2. Location-Conditioned Multimodal Retrieval and Explainability

We show additional visualization results of proposed location-conditioned multimodal retrieval on MIMIC-*loc*

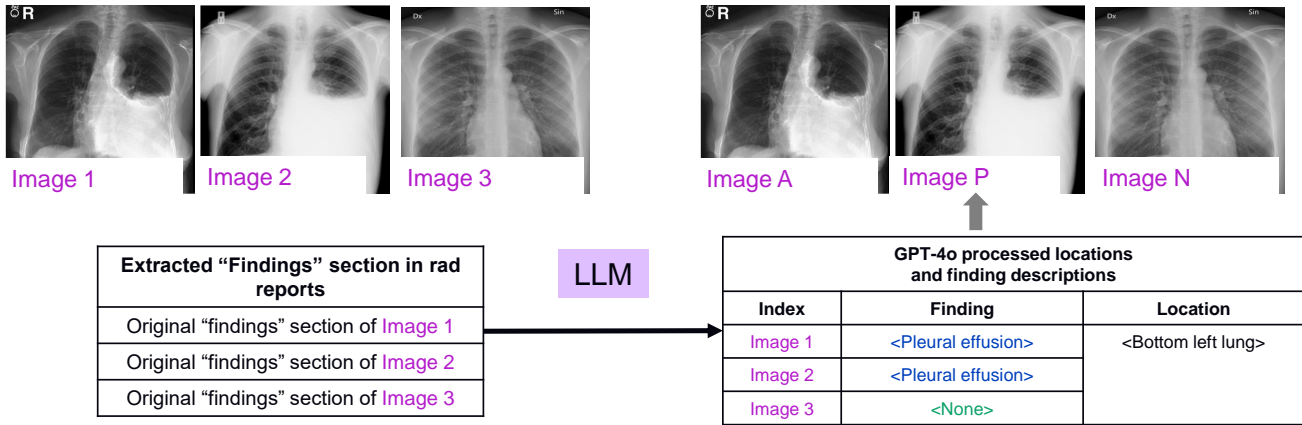


Figure 6. Illustration of the triplet sampling process for proposed location-conditioned contrastive learning. Image 1 and 2 are patient CXR images with “pleural effusion” at anatomical region “bottom left lung”. Image 3 shows a patient CXR image with normal lungs.

(*c.f.* Section 3.3 and 4.1 in the main paper) test set. We further demonstrate the explainability of the proposed ALC-ITR system in providing fine-level explainability and preliminary diagnosis. Visualizations are shown in Figure 9 and Figure 10.

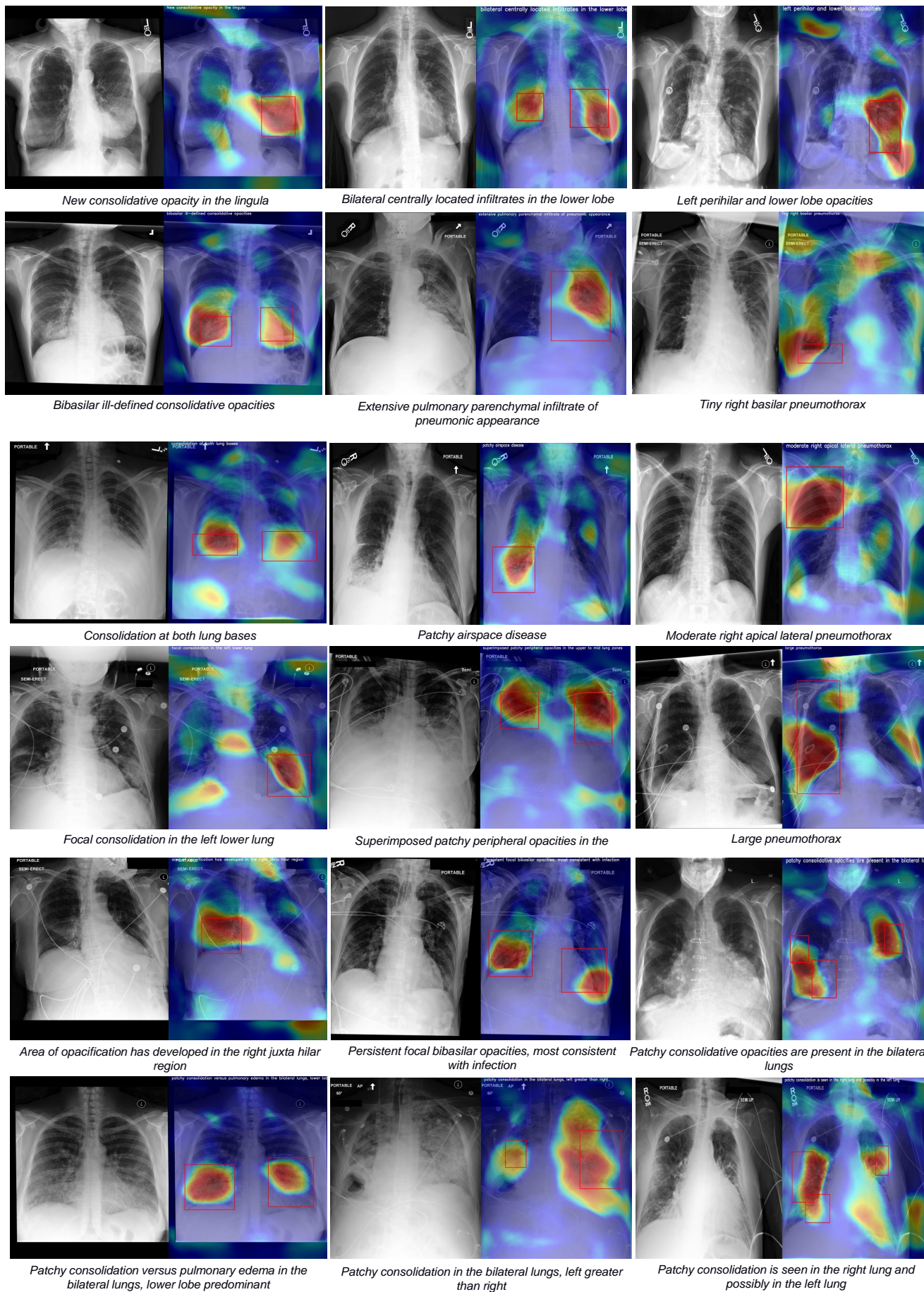


Figure 7. Visualization of phase grounding heatmaps of proposed RRA-VL on MS-CXR [3]. Red boxes are ground-truth bounding boxes.

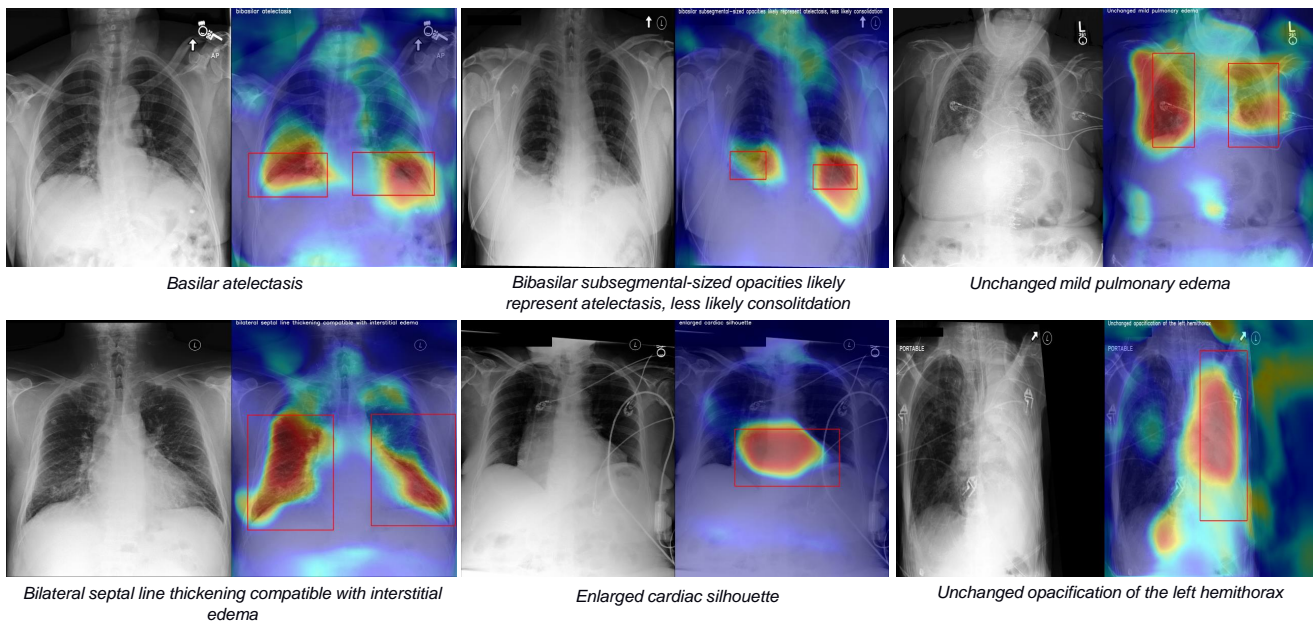
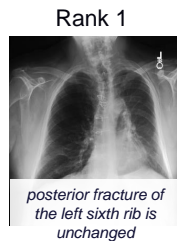
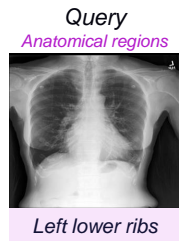
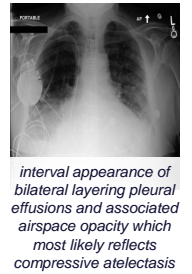
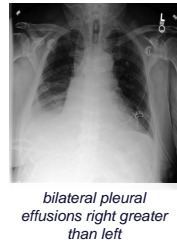


Figure 8. Visualization of phase grounding heatmaps of proposed RRA-VL on MS-CXR [3] (cont.). Red boxes are ground-truth bounding boxes.



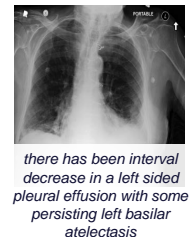
The visual similarity of the left lower rib area in the chest X-ray, along with the presence of a posterior fracture of the left sixth rib, suggests that the query patient may be experiencing rib trauma or possibly a rib contusion or hematoma, which could cause localized pain and discomfort. Further evaluation is needed to confirm the diagnosis and assess for any associated internal injuries.

*old healed left lower rib fractures are again noted*



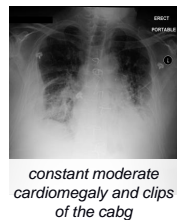
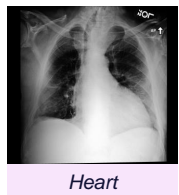
The bilateral pleural effusions, more pronounced on the right side, may indicate conditions such as heart failure, pneumonia, or malignancy, necessitating further evaluation to determine the underlying cause.

*moderate bilateral pleural effusions larger on the right than on the left are unchanged*



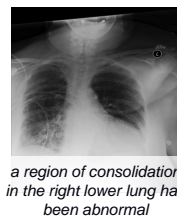
The presence of linear retrocardiac densities on the chest X-ray suggests the possibility of atelectasis, which may indicate underlying lung volume loss or collapse in that region, potentially due to factors such as obstruction or pleural effusion. Further evaluation is necessary to confirm the diagnosis and assess for any associated conditions.

*atelectasis is also within the differential*



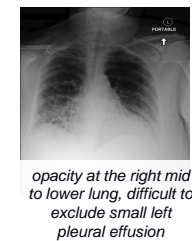
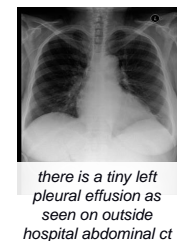
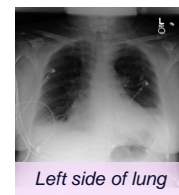
The patient likely has cardiomegaly associated with coronary artery disease, potentially requiring coronary artery bypass grafting (CABG) due to compromised heart function and structure. This condition suggests that the heart is enlarged due to increased workload or volume overload, likely from underlying ischemic heart disease.

*moderate to severe cardiomegaly is unchanged*



The findings on the Chest X-ray suggest the presence of a chronic pneumonia or an unresolved infection in the right lower lobe, which has shown improvement over time but still exhibits consolidation, indicating a need for further evaluation or management

*there is an extensive consolidation in the right lower lung probably in the right lower lobe*



The presence of a tiny left pleural effusion on the Chest X-ray, coupled with a prior abdominal CT, may suggest possible underlying conditions such as heart failure, infection, or malignancy. Further evaluation and correlation with clinical symptoms are necessary for a definitive diagnosis

*small to moderate left pleural effusion has increased slightly*



Figure 9. Visualization of generated explanations and preliminary diagnosis from our proposed ALC-ITR system. For each row, on the left we show one query CXR image with conditioned anatomical region (highlighted in purple boxes), retrieved top-1 and top-10 patient CXR image with report. On the right side, we show generated preliminary diagnosis (in black texts) and groundtruth disease/symptom descriptions (in purple texts) at the conditioned anatomical region accordingly.

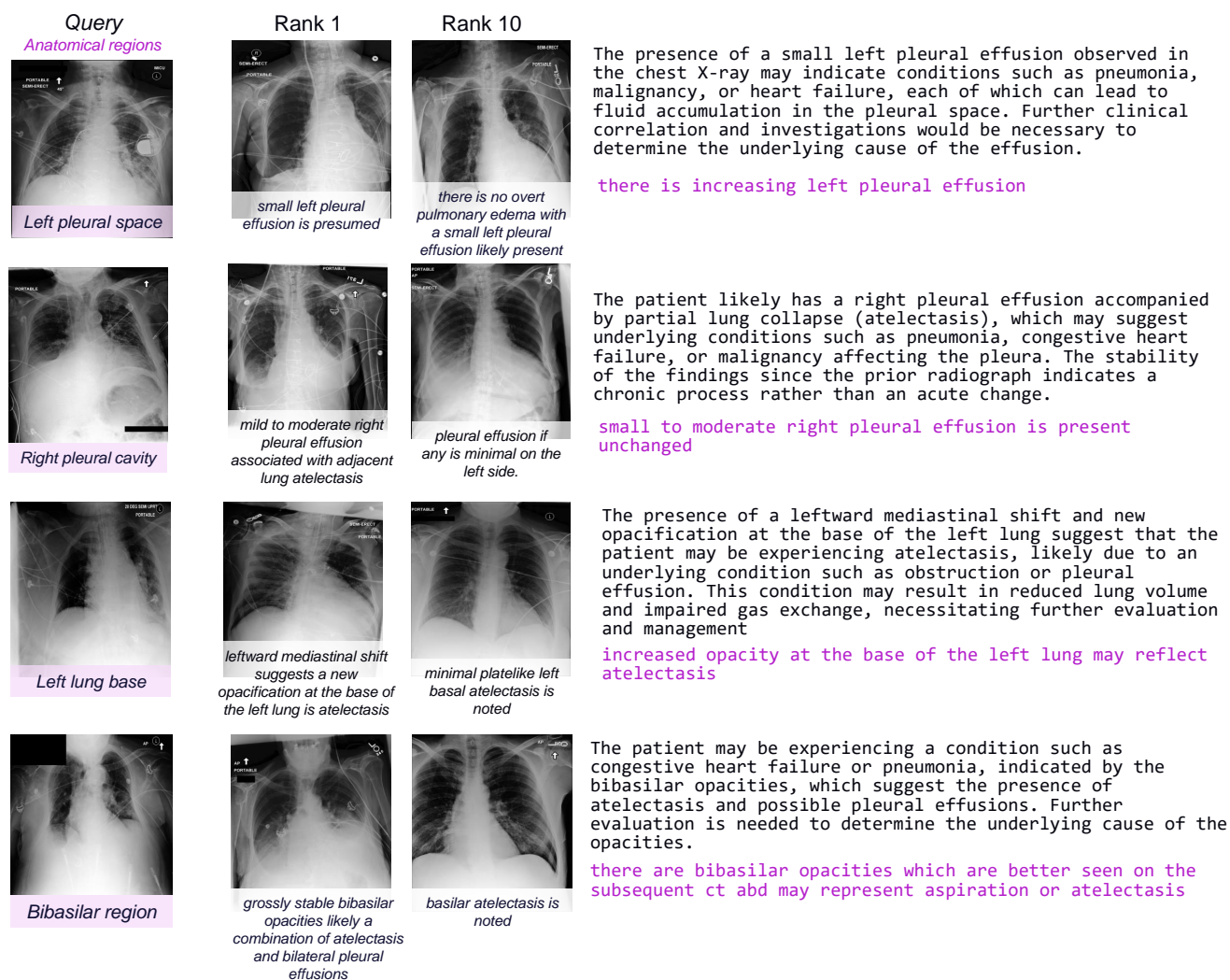


Figure 10. Visualization of generated explanations and preliminary diagnosis from our proposed ALC-ITR system (cont.).

## References

- [1] Josh Achiam, Steven Adler, Sandhini Agarwal, et al. Gpt-4 technical report. *arXiv:2303.08774*, 2023.
- [2] Emily Alsentzer, John Murphy, William Boag, Wei-Hung Weng, Di Jindi, Tristan Naumann, and Matthew McDermott. Publicly available clinical BERT embeddings. In *Proceedings of the 2nd Clinical Natural Language Processing Workshop*, 2019.
- [3] Benedikt Boecking, Naoto Usuyama, Shruthi Bannur, Daniel C. Castro, Anton Schwaighofer, Stephanie Hyland, Maria Wetscherek, Tristan Naumann, Aditya Nori, Javier Alvarez-Valle, Hoifung Poon, and Ozan Oktay. Making the most of text semantics to improve biomedical vision-language processing. In *ECCV*, 2022.
- [4] Minwoo Byeon, Beomhee Park, Haecheon Kim, Sungjun Lee, Woonhyuk Baek, and Saehoon Kim. Coyo-700m: Image-text pair dataset. <https://github.com/kakaobrain/coyo-dataset>, 2022.
- [5] Min Cao, Shiping Li, Juntao Li, Liqiang Nie, and Min Zhang. Image-text retrieval: A survey on recent research and development. In *IJCAI*, 2022.
- [6] Wenting Chen, Linlin Shen, Jingyang Lin, Jiebo Luo, Xiang Li, and Yixuan Yuan. Fine-grained image-text alignment in medical imaging enables explainable cyclic image-report generation. In *ACL (Volume 1: Long Papers)*, 2024.
- [7] Mengjun Cheng, Yipeng Sun, Long Wang, Xiongwei Zhu, Kun Yao, Jie Chen, Guoli Song, Junyu Han, Jingtuo Liu, Errui Ding, and Jingdong Wang. Vista: Vision and scene text aggregation for cross-modal retrieval. In *CVPR*, 2022.
- [8] Yuhao Cui, Zhou Yu, Chunqi Wang, Zhongzhou Zhao, Ji Zhang, Meng Wang, and Jun Yu. Rosita: Enhancing vision-and-language semantic alignments via cross- and intra-modal knowledge integration. In *ACM ICM*, 2021.
- [9] Gefen Dawidowicz, Elad Hirsch, and Ayellet Tal. Limitr: Leveraging local information for medical image-text representation. In *ICCV*, 2023.
- [10] Dina Demner-Fushman, Marc Kohli, Marc Rosenman, Sonya Shooshan, Laritza Rodriguez, Sameer Antani, George Thoma, and Clement McDonald. Preparing a collection of radiology examinations for distribution and retrieval. *Journal of the American Medical Informatics Association*, 23, 2015.
- [11] Jacob Devlin, Ming-Wei Chang, Kenton Lee, and Kristina Toutanova. BERT: pre-training of deep bidirectional transformers for language understanding. In *NAACL-HLT*, 2019.
- [12] Mark Endo, Rayan Krishnan, Viswesh Krishna, Andrew Y. Ng, and Pranav Rajpurkar. Retrieval-based chest x-ray report generation using a pre-trained contrastive language-image model. In *Proceedings of Machine Learning for Health*, pages 209–219, 2021.
- [13] Hao Fang, Saurabh Gupta, Forrest N. Iandola, Rupesh Kumar Srivastava, Li Deng, Piotr Dollár, Jianfeng Gao, Xiaodong He, Margaret Mitchell, John C. Platt, C. Lawrence Zitnick, and Geoffrey Zweig. From captions to visual concepts and back. *CVPR*, 2014.
- [14] Stephanie Fu, Mark Hamilton, Laura E. Brandt, Axel Feldmann, Zhoutong Zhang, and William T. Freeman. Featup: A model-agnostic framework for features at any resolution. In *ICLR*, 2024.
- [15] Tanmay Gupta, Arash Vahdat, Gal Chechik, Xiaodong Yang, Jan Kautz, and Derek Hoiem. Contrastive learning for weakly supervised phrase grounding. In *ECCV*, 2020.
- [16] Kaiming He, Xiangyu Zhang, Shaoqing Ren, and Jian Sun. Deep residual learning for image recognition. *arXiv:1512.03385*, 2015.
- [17] Brian Hu, Bhavan Vasu, and Anthony Hoogs. X-mir: Explainable medical image retrieval. In *WACV*, 2022.
- [18] Haoyang Huang, Yaobo Liang, Nan Duan, Ming Gong, Linjun Shou, Daxin Jiang, and Ming Zhou. Unicoder: A universal language encoder by pre-training with multiple cross-lingual tasks. In *EMNLP-IJCNLP*, 2019.
- [19] Shih-Cheng Huang, Liyue Shen, Matthew P. Lungren, and Serena Yeung. Gloria: A multimodal global-local representation learning framework for label-efficient medical image recognition. In *ICCV*, 2021.
- [20] Jeremy Irvin, Pranav Rajpurkar, Michael Ko, et al. Chexpert: a large chest radiograph dataset with uncertainty labels and expert comparison. In *AAAI*, 2019.
- [21] Zhanghexuan Ji, Mohammad Abuzar Shaikh, Dana Moukheiber, Sargur N Srihari, Yifan Peng, and Mingchen Gao. Improving joint learning of chest x-ray and radiology report by word region alignment. In *MLMI*, 2021.
- [22] Alistair E. W. Johnson, Tom J. Pollard, Lu Shen, Li wei H. Lehman, Mengling Feng, Mohammad Mahdi Ghassemi, Benjamin Moody, Peter Szolovits, Leo Anthony Celi, and Roger G. Mark. MIMIC-III, a freely accessible critical care database. *Scientific Data*, 3, 2016.
- [23] Junnan Li, Ramprasaath R. Selvaraju, Akhilesh Deepak Gotmare, Shafiq Joty, Caiming Xiong, and Steven Hoi. Align before fuse: Vision and language representation learning with momentum distillation. In *NeurIPS*, 2021.
- [24] Liunian Harold Li, Mark Yatskar, Da Yin, Cho-Jui Hsieh, and Kai-Wei Chang. Visualbert: A simple and performant baseline for vision and language. *ArXiv*, abs/1908.03557, 2019.
- [25] Zhongyu Li, Xiaofan Zhang, Henning Müller, and Shaoting Zhang. Large-scale retrieval for medical image analytics: A comprehensive review. *Medical Image Analysis*, 2018.
- [26] Ruizhi Liao, Daniel Moyer, Miriam Cha, Keegan Quigley, Seth Berkowitz, Steven Horng, Polina Golland, and William M. Wells. Multimodal representation learning via maximization of local mutual information. In *MICCAI*, 2021.
- [27] Bingqian Lin, Zicong Chen, Mingjie Li, Haokun Lin, Hang Xu, Yi Zhu, Jianzhuang Liu, Wenjia Cai, Lei Yang, Shen Zhao, Chenfei Wu, Ling Chen, Xiaojun Chang, Yi Yang, Lei Xing, and Xiaodan Liang. Towards medical artificial general intelligence via knowledge-enhanced multimodal pretraining. *arXiv preprint arXiv:2304.14204*, 2023.
- [28] Ilya Loshchilov and Frank Hutter. Decoupled weight decay regularization. In *International Conference on Learning Representations*, 2017.
- [29] Jiasen Lu, Dhruv Batra, Devi Parikh, and Stefan Lee. ViL-BERT: pretraining task-agnostic visiolinguistic representations for vision-and-language tasks. In *NeurIPS*, 2019.



- [30] Philip Müller, Georgios Kaissis, Congyu Zou, and Daniel Rueckert. Joint learning of localized representations from medical images and reports. In *ECCV*, 2022.
- [31] Philip Müller, Georgios Kaissis, and Daniel Rueckert. Chex: Interactive localization and region description in chest x-rays. In *ECCV*, 2024.
- [32] Zhengxin Pan, Fangyu Wu, and Bailing Zhang. Fine-grained image-text matching by cross-modal hard aligning network. In *CVPR*, 2023.
- [33] Konpat Preechakul, Chawan Piansaddhayanon, Burin Naowarat, Tirasan Khandhawit, Sira Sriswasdi, and Ekapol Chuangsuwanich. Set prediction in the latent space. In *NeurIPS*, 2021.
- [34] Adnan Qayyum, Syed Muhammad Anwar, Muhammad Awais, and Muhammad Majid. Medical image retrieval using deep convolutional neural network. *Neurocomputing*, 266: 8–20, 2017.
- [35] Leigang Qu, Meng Liu, Jianlong Wu, Zan Gao, and Liqiang Nie. Dynamic modality interaction modeling for image-text retrieval. In *SIGIR Conference on Research and Development in Information Retrieval*, 2021.
- [36] Alec Radford, Jong Wook Kim, Chris Hallacy, Aditya Ramesh, Gabriel Goh, Sandhini Agarwal, Girish Sastry, Amanda Askell, Pamela Mishkin, Jack Clark, Gretchen Krueger, and Ilya Sutskever. Learning transferable visual models from natural language supervision. In *ICML*, 2021.
- [37] Alec Radford, Jong Wook Kim, Chris Hallacy, Aditya Ramesh, Gabriel Goh, Sandhini Agarwal, Girish Sastry, Amanda Askell, Pamela Mishkin, Jack Clark, Gretchen Krueger, and Ilya Sutskever. Learning transferable visual models from natural language supervision. In *ICML*, 2021.
- [38] Christoph Schuhmann, Romain Beaumont, Richard Vencu, Cade Gordon, Ross Wightman, Mehdi Cherti, Theo Coombes, Aarush Katta, Clayton Mullis, Mitchell Wortsman, Patrick Schramowski, Srivatsa Kundurthy, Katherine Crowson, Ludwig Schmidt, Robert Kaczmarczyk, and Jenia Jitsev. Laion-5b: an open large-scale dataset for training next generation image-text models. In *NeurIPS*, 2022.
- [39] Constantin Seibold, Simon Reiß, M. Saquib Sarfraz, Rainer Stiefelhagen, and Jens Kleesiek. Breaking with fixed set pathology recognition through report-guided contrastive training. In *MICCAI*, 2022.
- [40] Weijie Su, Xizhou Zhu, Yue Cao, Bin Li, Lewei Lu, Furu Wei, and Jifeng Dai. VL-BERT: pre-training of generic visual-linguistic representations. In *ICLR*, 2020.
- [41] Tim Tanida, Philip Müller, Georgios Kaissis, and Daniel Rueckert. Interactive and explainable region-guided radiology report generation. In *CVPR*, 2023.
- [42] Tom van Sonsbeek and Marcel Worring. X-tra: Improving chest x-ray tasks with cross-modal retrieval augmentation. In *IPMI*, 2023.
- [43] Ashish Vaswani, Noam Shazeer, Niki Parmar, Jakob Uszkoreit, Llion Jones, Aidan N. Gomez, Łukasz Kaiser, and Illia Polosukhin. Attention is all you need. In *NeurIPS*, 2017.
- [44] Fuying Wang, Yuyin Zhou, Shujun Wang, Varut Vardhanabhuti, and Lequan Yu. Multi-granularity cross-modal alignment for generalized medical visual representation learning. In *NeurIPS*, 2022.
- [45] Zeqiang Wei, Kai Jin, and Xiuzhuang Zhou. Masked contrastive reconstruction for cross-modal medical image-report retrieval. *arXiv:2312.15840*, 2023.
- [46] Yang Yu, Peng Hu, Jie Lin, and Pavitra Krishnaswamy. Multimodal multitask deep learning for x-ray image retrieval. In *MICCAI*, 2021.
- [47] Yuhao Zhang, Hang Jiang, Yasuhide Miura, Christopher D. Manning, and C. Langlotz. Contrastive learning of medical visual representations from paired images and text. In *Machine Learning in Health Care*, 2022.